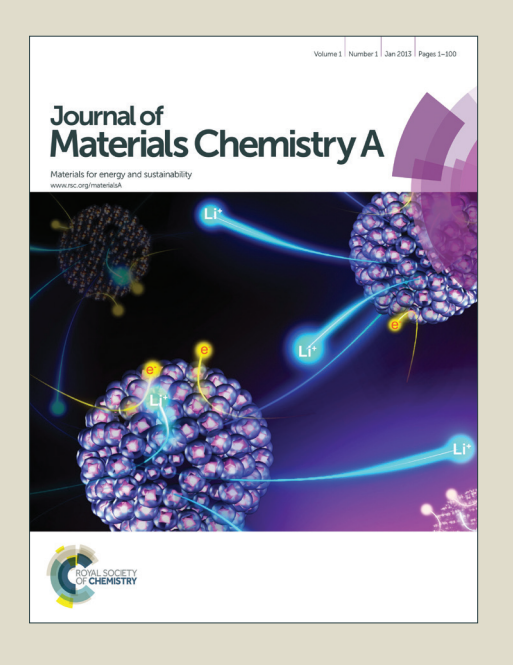
# Journal of Materials Chemistry A

Accepted Manuscript



This is an *Accepted Manuscript*, which has been through the Royal Society of Chemistry peer review process and has been accepted for publication.

Accepted Manuscripts are published online shortly after acceptance, before technical editing, formatting and proof reading. Using this free service, authors can make their results available to the community, in citable form, before we publish the edited article. We will replace this Accepted Manuscript with the edited and formatted Advance Article as soon as it is available.

You can find more information about *Accepted Manuscripts* in the **Information for Authors**.

Please note that technical editing may introduce minor changes to the text and/or graphics, which may alter content. The journal's standard <u>Terms & Conditions</u> and the <u>Ethical guidelines</u> still apply. In no event shall the Royal Society of Chemistry be held responsible for any errors or omissions in this *Accepted Manuscript* or any consequences arising from the use of any information it contains



# Construction of a photoanode with varied $TiO_2$ nanostructures for a Z907-sensitized solar cell with efficiency exceeding 10 %

Jia-Wei Shiu, Zih-Jian Lan, Chien-Yi Chan, Hui-Ping Wu and Eric Wei-Guang

Diau\*

Department of Applied Chemistry and Institute of Molecular Science, National Chiao

Tung University, No.1001, Ta Hsueh Rd., Hsinchu 30010, Taiwan;

e-mail: diau@mail.nctu.edu.tw

#### Abstract

For Z907-based dye-sensitized solar cells, we constructed photoanodes, layer by layer, containing titania nanostructures of varied types - spherical nanoparticles (NP), onedimensional nanorods (NR), and octahedron-like nanocrystals of varied size (HD1-HD3), in either a bi-layer (BL) or a multi-layer (ML) film configuration. To understand the kinetics of electron transport in these devices, we measured charge extraction, intensitymodulated photocurrent spectra and photovoltage spectra of devices made of either these nanomaterials or hybrid HD/NP composites (HDP). The HD devices featured an excellent characteristic of electron transport and upward-shifted potentials to produce V<sub>OC</sub> greater than those of the NP and NR devices, but the latter featured a larger dye loading to give J<sub>SC</sub> greater than for the former; the devices fabricated with hybrid HDP films showed enhanced  $J_{SC}$  and balanced  $V_{OC}$  to perform better than their individual counterparts. We constructed the ML devices based on the NP-BL system with additional HDP layers inserted between the two components, NP and SL, to enhance  $J_{\rm SC}$  so as to attain the best performance, with efficiency of power conversion (PCE) = 10.1 %, at film thickness (L) 26 µm. Because of the robust structural feature of the HD films, the devices fabricated with a simple BL film configuration, HD1/SL = 6/3, exhibited the best performance, PCE = 10.2% at  $L = 29 \mu m$ , which is a promising advance for Z907-based solar cells with a superior and enduring stability of performance for commercialization.

# Introduction

Dye-sensitized solar cells (DSSC) have attracted much attention because they present a highly promising alternative to conventional photovoltaic devices. <sup>1-3</sup> In such cells, dve molecules sensitize the surface of TiO<sub>2</sub> films to harvest solar energy. After absorption of light by the dye, electrons from the excited state of the dye are rapidly injected into the conduction band of TiO<sub>2</sub> and subsequently move toward the electrode. For a typical DSSC, the TiO<sub>2</sub> film is designed with a bi-layer (BL) configuration – a transparent TiO<sub>2</sub> active layer (AL) serves as a scaffold for dye adsorption and as a medium for electron transport; a scattering layer (SL) is added on top of the AL to enhance the light harvesting. 4-6 For an AL, anatase TiO<sub>2</sub> nanoparticles (NP) of size ~20 nm are employed to attain a dye loading (DL) of sufficient amount to harvest light in the visible spectral region; for a SL, particles of large size are introduced to enhance the light harvesting in the red and near-infrared region.<sup>5-8</sup> To improve the ability of the device to collect charge, various one-dimensional (1D) TiO<sub>2</sub> nanostructures – nanotubes, <sup>9,10</sup> nanowires, <sup>11, 12, 13</sup> nanofibers <sup>14</sup> and nanorods (NR)<sup>15-18</sup> – were developed, but these 1D titania nanostructures have typically smaller surface areas than their nanoparticle (NP)-based counterparts, which limit the DL on the TiO<sub>2</sub> surface from promoting further the device performance. One effective approach was to combine the 1D nanocrystals with conventional NP in a composite blend. 19,20 Alternatively, bi-functional hierarchical TiO<sub>2</sub> photoanodes were developed to combine both the DL ability and the effect of light scattering in one TiO<sub>2</sub> layer.<sup>21-25</sup>

Construction of an excellent TiO<sub>2</sub> photoanode for a high-performance DSSC requires a TiO<sub>2</sub> film with these important features: (i) a large specific surface area for sufficient DL, (ii) an excellent scattering effect for enhanced light harvesting, (iii) great crystallinality for rapid electron transport, and (iv) adequate porosity for feasible transport of the electrolyte in the mesoporous environment.<sup>4-7</sup> To fulfill these key factors in one single cell, Arakawa

Page 4 of 29

and co-workers reported a multi-layer (ML) configuration with  $TiO_2$  films containing small and large NP at varied mixing ratios that served as a working electrode for DSSC. <sup>26</sup> We proposed a hybrid  $TiO_2$  film with a NR-ML configuration for Z907-based solar cells. <sup>17</sup> The concept of our ML design was to add layers of 1D  $TiO_2$  nanorods of varied size (NR and LR) between the NP and SL of a conventional BL system for two reasons: first, the particle size increases gradually from the bottom layer (NP) to the top layer (SL), so that a suitable mesoporous network becomes available for electrolyte diffusion; second, the appropriate sequence of an energy cascade is established for feasible transport of electrons from SL, LR, NR to NP. <sup>17</sup> The thickness (*L*) of the  $TiO_2$  film with the NR-ML configuration is extensible to more than 30  $\mu$ m so that the Z907 device attained efficiency of power conversion PCE = 9.9 %, which was a promising advance for a sensitizer of this type with superior enduring stability. <sup>27</sup>

The aforementioned NR-ML film configuration involved both AL and SL for up to five components,<sup>17</sup> but fewer components would simplify the fabrication of the device for future commercialization of DSSC. For this purpose, we undertook a systematic approach to optimize, layer by layer, the device performance for TiO<sub>2</sub> photoanodes constructed according to a configuration either BL (2 components) or ML (3-4 components). Beyond the NP and NR materials, the promising octahedron-like titania nanocrystals (HD1-HD3)<sup>5</sup> are considered herein as key components of the AL to enhance the electron transport of the device. The Z907 devices with a four-component HDP-ML configuration attained the best PCE = 10.13 %, whereas those with a two-component HD1-BL configuration attained 10.21 %, which is a new record for Z907-sensitized solar cells.

#### **Results and Discussion**

Morphological and photovoltaic properties of varied TiO2 nanostructures

Figures 1a-1f display TEM images of six TiO<sub>2</sub> nanostructures – NP, NR, HD1, HD1.5, HD2 and HD3, that served as photoanode materials for DSSC. These TiO<sub>2</sub> nanocrystals were synthesized according to typical hydrothermal methods, reported elsewhere. <sup>4,5,17</sup> The spherical TiO2 NP was the same as the AL material used in a conventional DSSC with a BL configuration,<sup>4</sup> and the 1D NR was the key AL component in the device with a ML configuration reported previously. <sup>17</sup> For the octahedron-like HD nanocrystals, we showed the great photovoltaic performance of the devices made of these materials using N719 dye as a sensitizer: the HD devices featured remarkable open-circuit voltages ( $V_{\rm OC}$ ) because of their excellent electron-transport properties.<sup>5</sup> Here we first examined the photovoltaic performance of Z907 devices made of AL containing only one component – NP, NR, HD1, HD1.5, HD2 or HD3, at the same film thickness ( $L \sim 10 \mu m$ ) without SL. The J-Vcharacteristics and the IPCE spectra of those devices are shown in Fig. S1a and S1b, respectively, ESI; the corresponding DL and photovoltaic parameters are summarized in Table S1, ESI. We found a systematic trend of  $V_{OC}$  showing HD3 > HD2 > HD1.5 > HD1 > NR > NP, proving the superior crystallinity with larger crystals that increased  $V_{\rm OC}$ . In contrast, the trend of short-circuit current densities  $(J_{SC})$  was in the opposite direction, which is consistent with the trend of DL showing the same order. As a result, the overall efficiency ( $\eta$ ) of power conversion of the devices exhibited the same order as  $J_{SC}$  because of the dominating effect of DL.

Larger HD nanocrystals are reported to produce smaller specific surface areas for insufficient DL,<sup>5</sup> which is the reason for smaller  $J_{SC}$  and poorer  $\eta$  of HD devices relative to NP and NR devices. We therefore constructed hybrid TiO<sub>2</sub> films containing large HD nanocrystals (HD1.5, HD2 or HD3) and NP in a mass ratio 4/6, labeled HD1.5P, HD2P and HD3P for TiO<sub>2</sub> films HD1.5 + NP, HD2 + NP and HD3 + NP, respectively. Under the same experimental conditions ( $L \sim 10 \mu m$ ), the devices made of HD1.5P, HD2P and HD3P

films displayed  $J_{SC}$  and  $\eta$  (Figure S1 and Table S1, ESI) significantly better than their unblended counterparts. NP played a key role to enhance the DL of the hybrid films, but the compromise was a decreased  $V_{OC}$  of the devices. To understand the photovoltaic properties reflected by these TiO<sub>2</sub> films, we measured charge extraction (CE), intensity-modulated photocurrent spectra (IMPS) and intensity-modulated photovoltage spectra (IMVS) for these devices under five bias light intensities.<sup>28</sup> The results of the six devices made of the individual titania nanomaterials are shown in Figures 2a-2c and those made of the three HDP hybrid films are shown in Figures 2d-2f.

# Electron-transport properties of varied TiO<sub>2</sub> nanostructures

The electron-transport kinetics were derived from the IMPS measurements; the plots of diffusion coefficients of electrons (D) vs  $J_{SC}$  show a trend of diffusion with HD3 > HD2 > HD1.5 > HD1 ~ NR > NP (Figure 2a); for the HDP system, the plots of D vs  $J_{SC}$  show the order HD3P > HD2P > HD1.5P (Figure 2d). These results indicate that the transport of electrons in the HD films was more rapid than for the NR and NP films because the former were more crystalline than the latter. The size of the HD nanocrystals also plays a role in diffusion: we observed the systematic trend in Figure 2a with the capability of diffusion being almost equal between the HD1 and the NR films, but the variations of diffusion were much less in the hybrid HDP films. Figures 2b and 2e show the CE results for an opencircuit condition, giving a systematic trend for the TiO<sub>2</sub> potential shifts of the conduction band edge with order HD3 > HD2 > HD1.5 > HD1 > NR > NP and HD3P > HD2P > HD1.5P. The positions of the  $TiO_2$  potentials compared at the same electron densities ( $N_e$ ) are consistent with the variation of  $V_{\rm OC}$  listed in Table S1. Figures 2c and 2f show plots of electron lifetime  $(\tau_R)$  vs.  $N_e$  at the open-circuit condition obtained from the IMVS measurements. The charge recombination became more rapid when electron diffusion was more rapid. The magnitudes of V<sub>OC</sub> were controlled mainly by the positions of the TiO<sub>2</sub> potentials rather than by the retardation of charge recombination. These results are consistent with those reported for TiO<sub>2</sub> nanorods of varied length, <sup>17</sup> and support the conclusion that the devices with greater potentials possess more rapid electron diffusion and charge recombination.

#### Design of multi-layer film configurations: devices A-D

To enhance DL of the films with large HD nanocrystals, we constructed hybrid TiO<sub>2</sub> films with these nanomaterials in a ML configuration. Similar to the ML approach using NR as the AL, <sup>17</sup> we added 1-3 layers of HD1 or HD1.5 nanocrystals between TiO<sub>2</sub> NP (two layers) and large SL (three layers); the SL contains commercially available ST41 (Ishihara Sangyo Kaisha, Japan, particle size ~300 nm) mixed with NP in mass ratio ST41/NP = 80/20, the same as the SL-2 configuration reported previously. <sup>17</sup> As shown in Figure 3a, devices A-D were designed to have ML configurations with varied components of NR (three layers), HD1 (three layers), HD1 (two layers) + HD1.5 (one layer) and HD1.5 (three layers), respectively, with the total film thickness fixed at  $L \sim 28 \mu m$ . With Z907 dye as a sensitizer, the J-V curves and the IPCE action spectra are shown in Figures 3b and 3c, respectively. The corresponding film configurations, thicknesses and photovoltaic parameters are summarized in Table 1 with the average values derived from measurements of three devices fabricated under identical experimental conditions (raw data are listed in Table S2, ESI). The results indicate a systematic variation of device performance showing order A > B > C > D for  $J_{SC}$  and the opposite order for  $V_{OC}$ . The device with the NR-ML configuration (device A) consequently attained an overall performance ( $\eta = 9.7 \%$ ) slightly greater than that of devices with HD-ML configurations ( $\eta = 9.5$ -9.6 %). In the second phase, we therefore incorporated hybrid HDP films in varied layers in a HDP-ML configuration to enhance the DL of the films and to improve  $J_{SC}$  of the device.

#### HD/NP hybrid multi-layer film configuration: devices E-H

Similar to the idea of constructing high-performance ML films with a NR-ML or an HD-ML configuration, we inserted HDP films with varied layers between the two components in the NP-BL system with the configuration NP/SL = 2/3. Figure 4a shows the HDP-ML film configurations for devices E-H, for which L was systematically increased from 20 µm to 29 µm while the number of the HDP layers increased from one to four. The J-V curves and the IPCE action spectra of devices E-H are shown in Figures 4b and 4c, respectively; the corresponding parameters are summarized in Table 2 with the average values obtained from three identical devices (raw data are listed in Table S3, ESI). The device made of the hybrid HDP films with the HDP-ML configuration, NP/HD1.5P/HD2P/SL = 2/1/1/3, exhibited a device performance ( $\eta = 9.7$  %) similar to that of device A with a NR-ML configuration, but the film of the former (device E, L = 20 $\mu$ m) was thinner than that of the latter (device A,  $L = 27 \mu$ m). On increasing the contribution of HD2P in the HDP-ML films,  $J_{SC}$  increased whilst  $V_{OC}$  decreased until the film reached  $L=26 \mu m$ ; we obtained the best device performance for device G with  $\eta=9.9 \%$  in a 2/1/3/3 configuration. According to the IPCE spectra shown in Figure 4c, the enhanced  $J_{\rm SC}$ upon increasing the number of HD2P layers from device E to device G was due to the effect of scattering that increased the IPCE values at a wavelength greater than 600 nm. For device H, however, increasing the film thickness to 29 µm on adding one layer of HD2P decreased  $J_{SC}$  because of the decreased IPCE values in the region 400-600 nm, which gave a poorer overall performance for device H than for device G.

#### **HD-based bi-layer film configuration: devices I-M**

We examined also the performance of a device with a simple BL configuration, HD1/SL. In such an HD1-BL system, the number of SL was fixed at three and the number of HD1 layers was varied from 3 to 7, for which the film thickness increased from 20 μm to 32 μm; the corresponding HD1-BL film configurations to fabricate devices I-M are

shown in Figure 5a. The *J-V* curves appear in Figure 5b and the IPCE action spectra of devices I-M in Figure 5c. The corresponding photovoltaic parameters are summarized in Table 3 (the raw data are tabulated in Table S4, ESI). The superior crystallinity of the HD1 nanocrystals gave the excellent performance shown here. In particular,  $V_{OC}$  attained 779 mV for device I at  $L = 20 \mu m$  and decreased by only 20 mV for device M at  $L = 32 \mu m$ , but the amount of DL was significantly increased upon increasing the number of HD1 layers. Accordingly,  $J_{SC}$  increased from 16.60 mA cm<sup>-2</sup> (device I) to 17.75 mA cm<sup>-2</sup> (device L), and then slightly decreased to 17.56 mA cm<sup>-2</sup> (device M) at  $L = 32 \mu m$ . Figure 5c displays the IPCE spectra of these devices showing a systematic trend on the light-harvesting feature at wavelength greater than 600 nm upon increasing the number of the HD1 layers, which is consistent with the variation of  $J_{SC}$  from device I to device L; the slight decrease of  $J_{SC}$  of device M is due to the decreased IPCE values at wavelength smaller than 500 nm. The best performance for devices of this series hence appeared at device L with the film configuration HD1/SL = 6/3, for which the efficiency  $\eta$  attained 9.9%, similar to the performance of device G with a HDP-ML configuration.

Figures 6a-6d show plots of the photovoltaic parameters,  $J_{SC}$ ,  $V_{OC}$ , FF and  $\eta$ , respectively, as a function of L to compare the performances between the HDP-ML and the HD1-BL devices. The advantage of the HDP-ML films is the amount of DL, which gave a larger  $J_{SC}$  for the HDP-ML devices than for the HD1-BL devices compared at the same L. In contrast, the advantage of the HD1-BL films is the crystallinity of the nanocrystals, which gave larger  $V_{OC}$  for the HD1-BL devices than for the HDP-ML devices compared at the same L. The best performance of the HDP-ML devices occurred at  $L=26~\mu m$  (device G), compared with HD1-BL at  $L=29~\mu m$  (device L); both attained  $\eta=9.9~\%$ . We therefore further optimized the device performance for both devices G and L with twenty cells of each configuration.

### Performance optimization for devices G and L

We optimized device G with a film configuration of HDP-ML (NP/HD1.5P/HD2P/SL = 2/1/3/3) and for device L with a film configuration of HD1-BL (HD1/SL = 6/3). In total, 20 identical devices for each film configuration were fabricated according to the same experimental procedure under the optimal conditions. The resulting photovoltaic parameters of devices G and L are listed in Tables S5 and S6, respectively. For device G, the twenty  $\eta$  values are distributed between 9.85 % and 10.15 % with average value  $10.00\pm0.06$  %; for device L, the twenty  $\eta$  values are distributed between 9.87 % and 10.21 % with average value  $10.03\pm0.08$  %. Figure 7a shows histograms of distributions of efficiencies of power conversion of devices G, and Figure 7b for L, for the counts of the devices with PCE in a step 0.05 %. The best performance, of device G, featured  $J_{SC}$ /mA cm<sup>-2</sup> = 18.63,  $V_{OC}$ /mV = 752, FF = 0.723 and  $\eta$  = 10.13 %, and that of device L featured  $J_{SC}$ /mA cm<sup>-2</sup> = 17.88,  $V_{OC}$ /mV = 758, FF = 0.753 and  $\eta$  = 10.21 %. Devices of both types HDP-ML and HD1-BL with PCE exceeding 10 % were fabricated with a Z907 dye, which exhibit an outstanding enduring stability of performance to match the industrial standard for outdoor applications.<sup>27</sup>

### Enduring stability of performance for device L

Because of the remarkable performance of device L, we conducted a long-term stability test for device L under varied experimental conditions over a period 1435 h; the corresponding photovoltaic performances are shown in Figure 8. In the first stage, the cell was stored in darkness at ~20 °C for 1022 h. During this period, the device performance increased slowly from  $\eta = 9.1$  % in the beginning (0 h) to  $\eta = 10.0$  % at 256 h; it then maintained a constant performance ( $\eta = 10.0$ -10.2 %) during the period 300-1000 h. For the second stage, the cell was heated to 60 °C under one-sun irradiation during the period 1022-1223 h; the  $V_{\rm OC}$  and FF values of the device slightly decreased and the device

efficiency decreased to  $\eta$  = 9.1 % at 1096 h but remained steady under this condition. We then raised the temperature of the cell to 70 °C under one-sun irradiation during the period 1223-1344 h; the device performance decreased only slightly under these conditions. The final stage began at 1344 h; the device temperature was increased to 80 °C under one-sun irradiation until the performance degraded significantly at the end of the test, 1435 h. As temperature 80 °C is near the boiling point of the solvent (acetonitrile) applied for the electrolyte, we expected that the cell would deteriorate rapidly under these conditions. Nevertheless, our results indicate that the best performed device L has superior enduring stability of performance in the dark as well as under one-sun illumination for a temperature below 70 °C. More severe light-soaking conditions might be applied for this system with other electrolytes; work is in progress along this direction.

# Conclusion

According to a systematic approach, layer by layer, we designed, fabricated and characterized a titania photoanode with a bi-layer (BL) or multi-layer (ML) film configuration for highly efficient dye-sensitized solar cells using Z907 dye as a photosensitizer. The components in the BL or ML films contained various  $TiO_2$  nanostructures including conventional nanoparticles (NP), one-dimensional nanorods (NR), or octahedron-like nanocrystals of varied sizes (HD1, HD1.5, HD2 and HD3); their kinetics of electron transport and charge recombination were well characterized with techniques CE, IMPS and IMVS. Figure 9 displays the film configurations that attained the best device performance for each system. We demonstrated  $^{17}$  that the Z907 device in a NR-ML system with a complicated film configuration, NP/NR/LR/SL-1/SL-2 = 2/3/1/1/2, attained the best performance  $\eta = 9.91$  % at film thickness L = 26  $\mu$ m. The HD/NP hybrid films exhibited a great flexibility to accommodate both effects of large dye loading (via NP) and rapid

electron transport (via HD) in a ML configuration (HDP-ML) well designed. As a result, the best device performance occurred at film configuration NP/HD1.5P/HD2P/SL = 2/1/3/3 (device G), giving the best PCE 10.13 %, which is slightly improved with respect to that of the NR-ML system at the same film thickness ( $L = 26 \mu m$ ). The devices made of a conventional NP-BL system attained the best performance,  $\eta = 9.31$  % at L = 19 µm, of which the delicate nature of the NP films at larger L precludes further improvement. In contrast, the robust mechanical feature of the HD films enabled us to make thicker films to enhance DL and  $J_{SC}$  for the HD1-BL system, for which the best performance  $\eta = 10.21$  % was obtained at L = 29 µm with a bi-layer film configuration, HD1/SL = 6/3 (device L). Twenty identical devices were fabricated under the same experimental conditions for each promising system; average efficiencies 10.00±0.06 % and 10.03±0.08 % were obtained for devices G and L, respectively. The Z907 dye exhibits excellent thermal stability but suffers from small absorption coefficients. The devices made of Z907 dye have been fully optimized based on our approach, with either a simple bi-layer or a complex multi-layer film configuration, to attain PCE exceeding 10 % for more than 1000 h under varied experimental conditions, indicating prospective commercialization of DSSC in the near future.

#### **Experiments**

#### **Device fabrication**

The DSSC devices were fabricated with a titania working electrode and a Pt-coated counter electrode in a structure of sandwich type. For the working electrode, varied  $TiO_2$  nanostructures – NP, NR and HD1-HD3 – were synthesized with hydrothermal methods reported elsewhere; 4.5.17 ethyl cellulose and  $\alpha$ -terpineol were added to the ethanol solution of these  $TiO_2$  nanostructures to prepare a viscous paste suitable for screen printing. <sup>29</sup> The

TiO<sub>2</sub> paste was then coated onto a TiCl<sub>4</sub>-treated FTO glass substrate (TEC 7, Hartford, USA) to obtain a film of the required thickness (active size 0.4×0.4 cm<sup>2</sup>) with repetitive screen printing. The annealing temperature was kept at 125 °C for 6 min for each layer; the film thickness of a typical screen-printing layer was 3-4 μm. The TiO<sub>2</sub> films, as prepared according to either a ML or a BL configuration to fabricate devices A-M, were annealed according to a programmed procedure: heating at 80 °C for 15 min, at 135 °C for 10 min, at 325 °C for 30 min, at 375 °C for 5 min, at 450 °C for 15 min, and at 500 °C for 15 min. The annealed films were treated with fresh TiCl<sub>4</sub> aqueous solution (40 mM) at 70 °C for 30 min and sintered at 500 °C for 30 min. The dye uptake on these TiO<sub>2</sub> films was performed in a solution (Z907 dye, 3×10<sup>-4</sup> M) containing chenodeoxycholic acid (CDCA, 3×10<sup>-4</sup> M) in an equi-volume mixture of acetonitrile and tert-butanol at 25 °C for 3-5 h. The counter electrode was made on spin-coating the H<sub>2</sub>PtCl<sub>6</sub>/isopropanol solution onto a FTO glass substrate through a typical thermal decomposition.<sup>30</sup> The two electrodes were assembled into a cell of sandwich type and sealed with a spacer of thickness 40 µm. The electrolyte injected into the device contained GuNCS (0.1 M), I<sub>2</sub> (0.03 M), LiI (0.05 M), PMII (1.0 M), 4-t-butylpyridine (0.5 M) in acetonitrile.

#### Film and device characterizations

We investigated the morphologies of the various TiO<sub>2</sub> nanostructures with a high-resolution transmission electron microscope (HRTEM, JEM-2100, JEOL). The current-voltage (*J*–*V*) characteristics of the DSSC devices covered with a black mask (aperture area 0.2025 cm<sup>2</sup>) were determined with a solar simulator (AM 1.5G, XES-40S1, SAN-EI). The spectra of incident photon-to-current conversion efficiency (IPCE) of the corresponding devices were measured with a system comprising a Xe lamp (A-1010, PTi, 150 W), monochromator (PTi, 1200 gr mm<sup>-1</sup> blazed at 500 nm) and source meter (Keithley 2400).

The charge extraction (CE), intensity-modulated photocurrent (IMPS) and photovoltage (IMVS) spectra were measured with CIMPS instruments (Zahner) reported elsewhere.<sup>28</sup>

**Electronic Supplementary Information (ESI)** available: Figure S1 and Tables S1-S6.

**Acknowledgements.** We acknowledge Ministry of Science and Technology of Taiwan and Ministry of Education of Taiwan for the support of this project.

# **References**

- 1. A. Hagfeldt, G. Boschloo, L. Sun, L. Kloo and H. Pettersson, *Chem. Rev.*, 2010, **110**, 6595-6663.
- 2. N. Tétreault and M. Grätzel, *Energy Environ. Sci.*, 2012, **5**, 8506-8516.
- 3. L.-L. Li and E. W.-G. Diau, *Chem. Soc. Rev.*, 2013, **42**, 291-304.
- 4. S. Ito, T. N. Murakami, P. Comte, P. Liska, C. Grätzel, M. K. Nazeeruddin and M. Grätzel, *Thin Solid Films*, 2008, **516**, 4613-4619.
- 5. J.-W. Shiu, C.-M. Lan, Y.-C. Chang, H.-P. Wu, W.-K. Huang and E. W.-G. Diau, *ACS Nano*, 2012, **6**, 10862-10873.
- 6. C.-M. Lan, S.-E. Liu, J.-W. Shiu, J.-Y. Hu, M.-H. Lin and E. W.-G. Diau, *RSC Advances*, 2013, **3**, 559-565.
- 7. H. J. Koo, J. Park, B. Yoo, K. Yoo, K. Kim and N. G. Park, *Inorg. Chim. Acta*, 2008, **361**, 677-683.
- 8. Q. F. Zhang, D. Myers, J. L. Lan, S. A. Jenekhe and G. Z. Cao, *Phys. Chem. Chem. Phys.*, 2012, **14**, 14982-14998.
- 9. L.-L. Li, C.-Y. Tsai, H.-P. Wu, C.-C. Chen and E. W.-G. Diau, *J. Mater. Chem.*, 2010, **20**, 2753-2758.
- 10. L.-L. Li, Y.-J. Chen, H.-P. Wu, N. S. Wang and E. W.-G. Diau, *Energy Environ. Sci.*, 2011, **4**, 3420-3425.
- 11. Z. J. Zhou, J. Q. Fan, X. Wang, W. H. Zhou, Z. L. Du and S. X. Wu, *ACS Appl. Mater. Interfaces*, 2011, **3**, 4349-4353.
- 12. D. H. Kim, W. M. Seong, I. J. Park, E.-S. Yoo, S. S. Shin, J. S. Kim, H. S. Jung, S. Lee and K. S. Hong, *Nanoscale*, 2013, **5**, 11725–11732.
- 13. Y. Bai, H. Yu, Z. Li, R. Amal, G. Q. (Max) Lu, and L. Wang, *Adv. Mater.*, 2012, **24**, 5850–5856.
- 14. J.-Y. Liao, J.-W. He, H. Xu, D.-B. Kuang and C.-Y. Su, *J. Mater. Chem.*, 2012, **22**, 7910-7918.
- 15. J. Jiu, S. Isoda, F. Wang and M. Adachi, *J. Phys. Chem. B*, 2006, **110**, 2087-2092.
- 16. G. Melcarne, L. D. Marco, E. Carlino, F. Martina, M. Manca, R. Cingolani, G. Gigli and G. Ciccarella, *J. Mater. Chem.*, 2010, **20**, 7248-7254.

- 17. H.-P. Wu, C.-M. Lan, J.-Y. Hu, W.-K. Huang, J.-W. Shiu, Z.-J. Lan, C.-M. Tsai, C.-H. Su and E. W.-G. Diau, *J. Phys. Chem. Lett.*, 2013, **4**, 1570-1577.
- 18. H. S. Han, J. S. Kim, D. H. Kim, G. S. Han, H. S. Jung, J. H. Noh and K. S. Hong, *Nanoscale*, 2013, **5**, 3520–3526.
- 19. R. Mohammadpour, A. I. zad, A. Hagfeldt and G. Boschloo, *Phys. Chem. Chem. Phys.*, 2011, **13**, 21487-21491.
- 20. J. Sheng, L. Hu, S. Xu, W. Liu, L. Mo, H. Tian and S. Dai, *J. Mater. Chem.*, 2011, **21**, 5457-5463.
- 21. J. Y. Liao, B. X. Lei, D. B. Kuang and C. Y. Su, *Energy Environ. Sci.*, 2011, **4**, 4079-4085.
- 22. F. Sauvage, D. Chen, P. Comte, F. Huang, L.-P. Heiniger, Y.-B. Cheng, R. A. Caruso and M. Gräetzel, *ACS Nano*, 2010, **4**, 4420-4425.
- 23. D. Chen and R. A. Caruso, *Adv. Funct. Mater.*, 2013, **23**, 1356-1374.
- 24. S. S. Mali, H. Kim, C. S. Shim, P. S. Patil, J. H. Kim and C. K. Hong, *Scientific Reports*, 2013, **3**, doi:10.1038/srep03004.
- 25. D. K. Roh, J. A. Seo, W. S. Chi, J. K. Koh and J. H. Kim, *J. Mater. Chem.*, 2012, **22**, 11079–11085.
- Z.-S. Wang, H. Kawauchi, T. Kashima and H. Arakawa, *Coord. Chem. Rev.*, 2004, 248, 1381-1389.
- 27. P. Wang, S. M. Zakeeruddin, J. E. Moser, M. K. Nazeeruddin, T. Sekiguchi and M. Grätzel, *Nat. Mater.*, 2003, **2**, 402-407.
- 28. L.-L. Li, Y.-C. Chang, H.-P. Wu and E. W.-G. Diau, *Int. Rev. Phys. Chem.*, 2012, **31**, 420-467.
- 29. S. Ito, P. Chen, P. Comte, M. K. Nazeeruddin, P. Liska, P. Péchy and M. Grätzel, *Prog. Photovoltaics Res. Appl.*, 2007, **15**, 603-612.
- 30. L.-L. Li, C.-W. Chang, H.-H. Wu, J.-W. Shiu, P.-T. Wu and E. W.-G. Diau, *J. Mater. Chem.*, 2012, **22**, 6267-6273.

**Table 1.** Photovoltaic parameters of devices made of Z907 dye and multi-layer (ML)  $TiO_2$  films (total film thickness L) with varied film configurations defined as A-D under simulated AM-1.5G illumination (power density 100 mW cm<sup>-2</sup>) and active area 0.16 cm<sup>2</sup> with a black mask of area 0.2025 cm<sup>2</sup>.

Device	TiO <sub>2</sub> film	L	$J_{ m SC}$	$V_{\rm OC}$	FF	η
	configuration	/µm	/mA cm <sup>-2</sup>	/mV	rr	/%
A	2/ <b>3</b> /3 <sup>b</sup>	27	17.98±0.11	748±2	0.718±0.005	9.67±0.02
В	2/ <b>3</b> /3 <sup>c</sup>	28	17.57±0.05	754±2	0.722±0.003	9.56±0.06
C	2/ <b>2/1</b> /3 <sup>d</sup>	28	17.43±0.04	756±0	0.722±0.002	9.51±0.00
D	2/ <b>3</b> /3 <sup>e</sup>	28	17.01±0.10	765±0	0.735±0.003	9.56±0.02

<sup>&</sup>lt;sup>a</sup> Photovoltaic parameters are average values obtained from analysis of *JV* curves of three identical working electrodes (Table S2, ESI). <sup>b</sup> The TiO<sub>2</sub> film has the ML configuration NP/NR/SL. <sup>c</sup> The TiO<sub>2</sub> film has the ML configuration NP/HD1/SL. <sup>d</sup> The TiO<sub>2</sub> film has the ML configuration NP/HD1.5/SL. <sup>e</sup> The TiO<sub>2</sub> film has the ML configuration NP/HD1.5/SL.

**Table 2.** Photovoltaic parameters of devices made of Z907 dye and multi-layer (ML)  $TiO_2$  films (total film thickness L) with varied film configurations defined as E-H under simulated AM-1.5G illumination (power density 100 mW cm<sup>-2</sup>) and active area 0.16 cm<sup>2</sup> with a black mask of area 0.2025 cm<sup>2</sup>.

Device	TiO <sub>2</sub> film	L	$J_{ m SC}$	$V_{\rm OC}$	FF	η
	configuration <sup>b</sup>	/µm	/mA cm <sup>-2</sup>	/mV		/%
Е	2/1/1/3	20	17.24±0.11	758±0	0.743±0.006	9.71±0.02
F	2/1/ <b>2</b> /3	24	17.84±0.16	752±2	0.732±0.008	9.82±0.05
G	2/1/ <b>3</b> /3	26	18.17±0.13	749±0	0.727±0.002	9.89±0.06
Н	2/1/ <b>4</b> /3	29	17.45±0.08	743±1	0.743±0.004	9.66±0.05

<sup>&</sup>lt;sup>a</sup> Photovoltaic parameters are average values obtained from analysis of *JV* curves of three identical working electrodes (Table S3, ESI). <sup>b</sup> The TiO<sub>2</sub> films have the ML configuration NP/HD1.5P/HD2P/SL with layers of HD2P of varied number.

**Table 3.** Photovoltaic parameters of devices made of Z907 dye and  $TiO_2$  films (total film thickness L) with HD1/SL bi-layer (BL) configuration defined as I-M under simulated AM-1.5G illumination (power density 100 mW cm<sup>-2</sup>) and active area 0.16 cm<sup>2</sup> with a black mask of area 0.2025 cm<sup>2</sup>.

Device	TiO <sub>2</sub> film	L	$J_{ m SC}$	$V_{\rm OC}$	FF	η
	configuration <sup>b</sup>	/µm	/mA cm <sup>-2</sup>	/mV		/%
I	<b>3</b> /3	20	16.60±0.07	779±2	0.747±0.001	9.66±0.03
J	<b>4</b> /3	23	16.99±0.14	775±1	0.741±0.004	9.76±0.04
K	<b>5</b> /3	26	17.36±0.10	768±2	0.737±0.003	9.83±0.03
L	<b>6</b> /3	29	17.75±0.07	760±2	0.736±0.003	9.92±0.01
M	<b>7</b> /3	32	17.56±0.15	757±1	0.743±0.006	9.87±0.01

<sup>&</sup>lt;sup>a</sup> Photovoltaic parameters are average values obtained from analysis of *JV* curves of three identical working electrodes (Table S4, ESI). <sup>b</sup> The TiO<sub>2</sub> films have the BL configuration HD1/SL with varied number of layers of HD1.

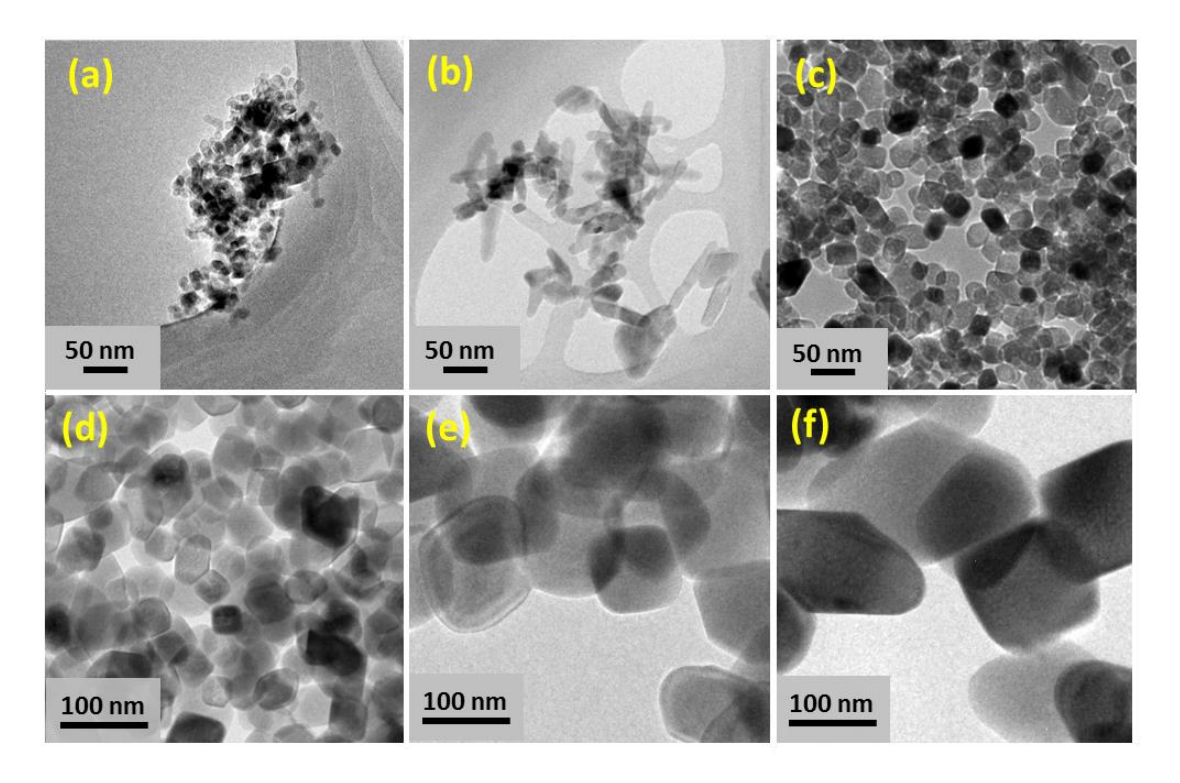


**Figure 1.** TEM images of varied TiO<sub>2</sub> nanostructures (a) NP, (b) NR, (c) HD1, (d) HD1.5, (e) HD2 and (f) HD3.

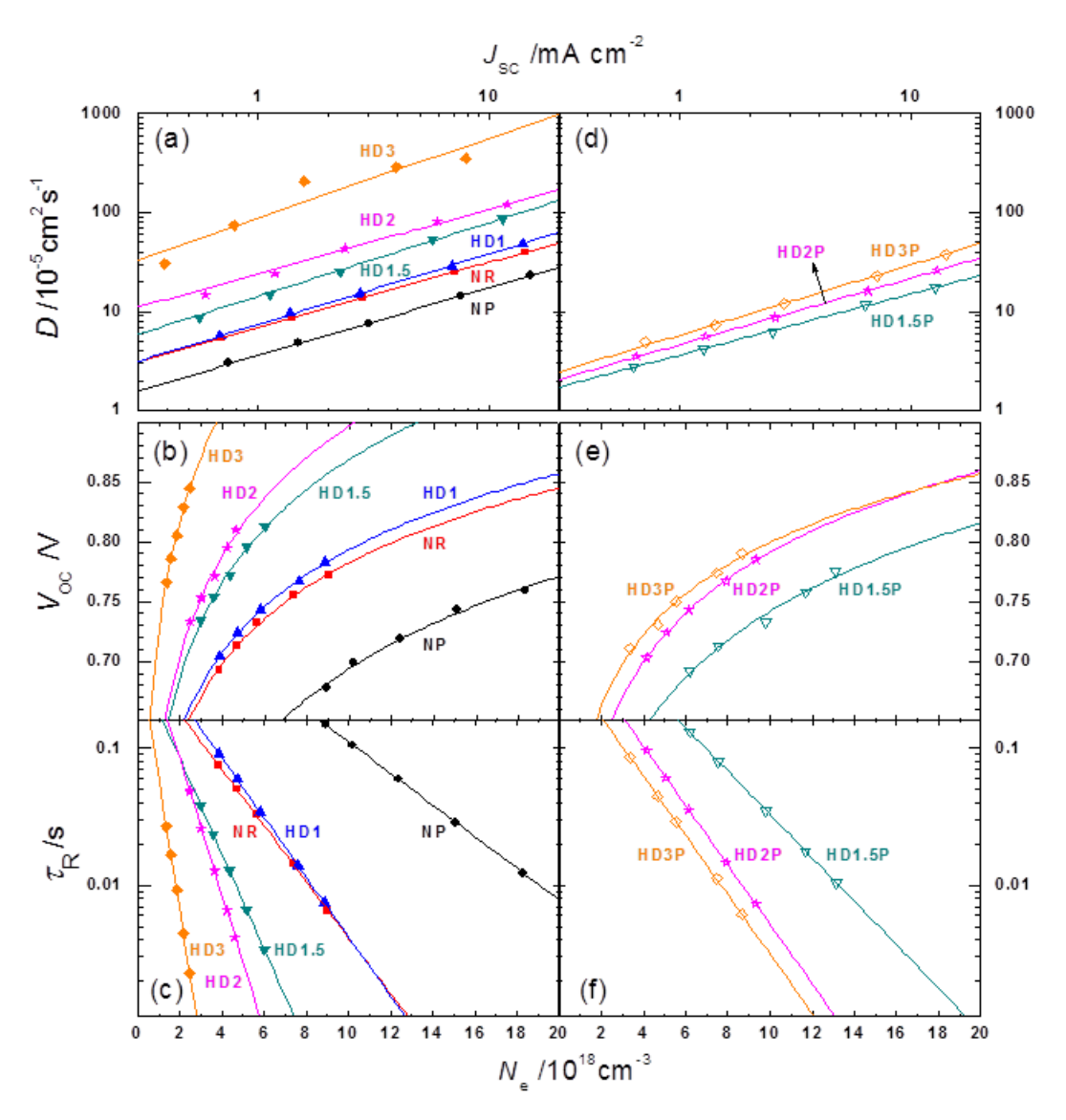
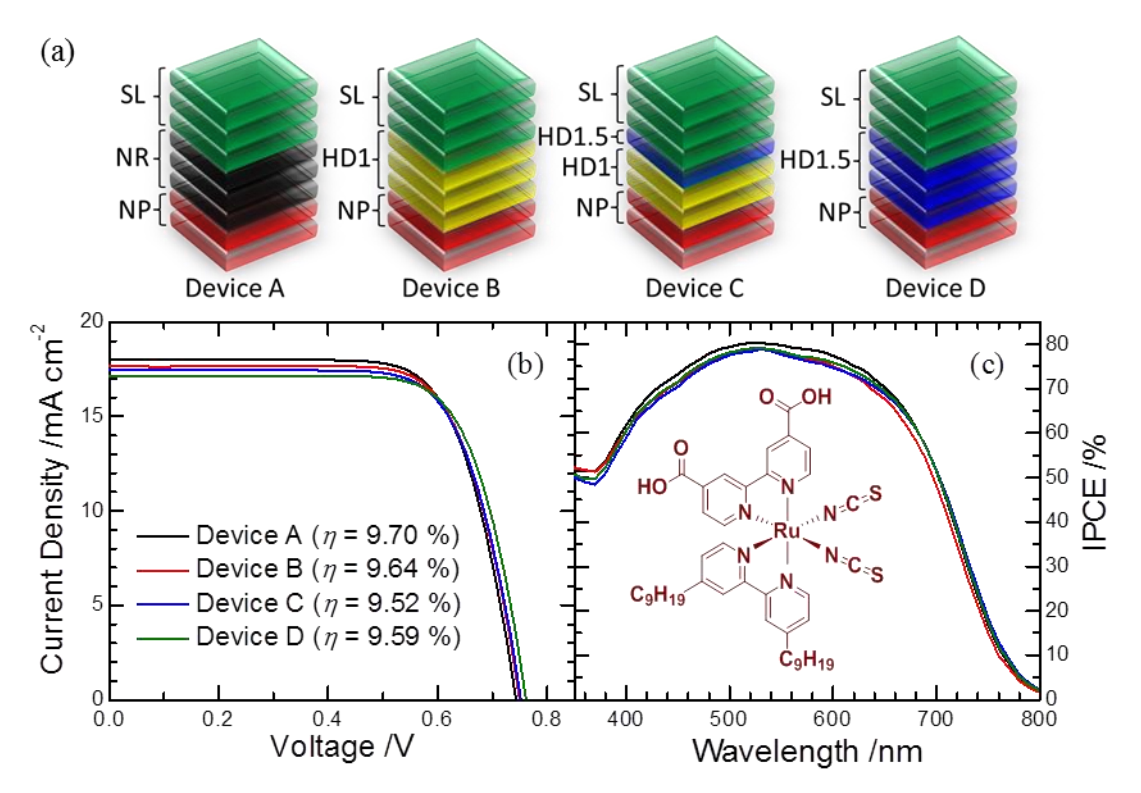
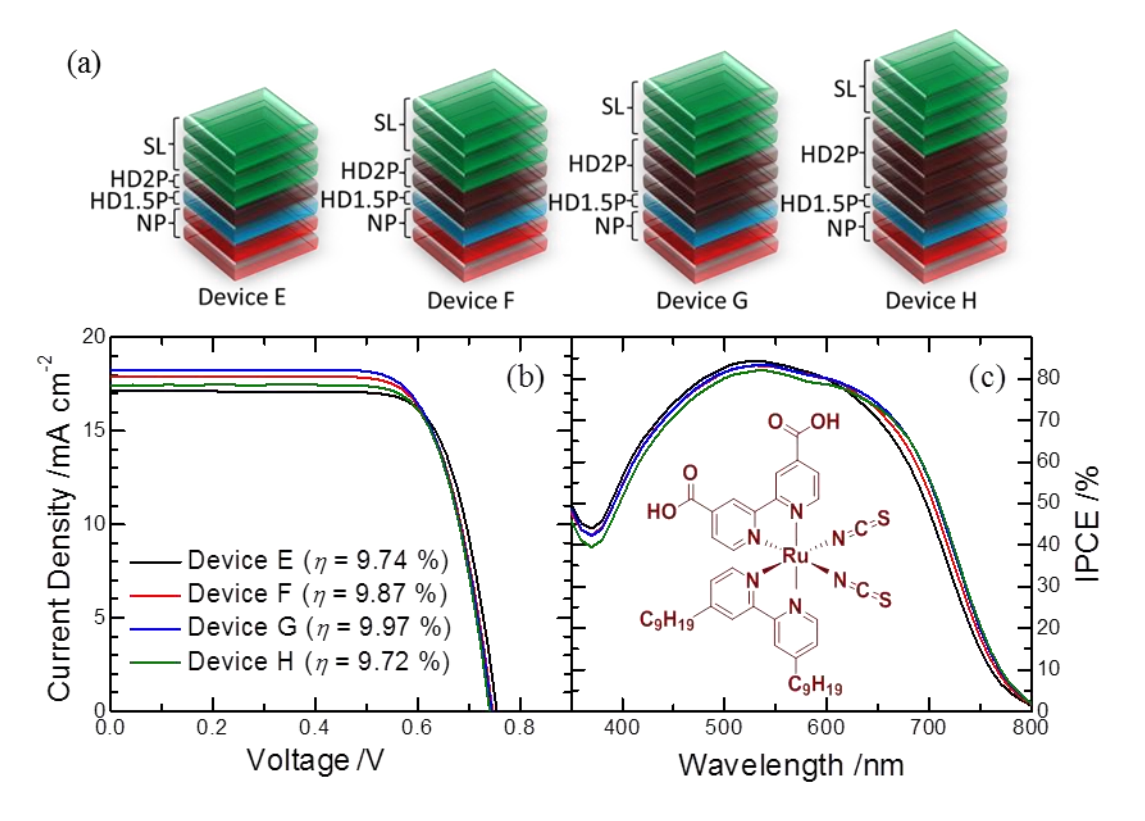


Figure 2. Characteristic plots of electron transport obtained from CE, IMPS and IMVS measurements for devices made of various  $TiO_2$  nanostructures at film thickness  $L \sim 10 \mu m$ : (a)-(c) for NP, NR, HD1, HD1.5, HD2 and HD3; (d)-(f) for HD1.5P, HD2P and HD3P. (a) and (d) are plots of electron diffusion coefficient (*D*) vs.  $J_{SC}$ , (b) and (e) are plots of  $V_{OC}$  vs. charge density ( $N_e$ ), and (c) and (f) are plots of electron lifetime ( $\tau_R$ ) vs.  $N_e$ .



**Figure 3.** Photovoltaic characteristic plots of (b) JV curves and (c) IPCE action spectra for devices A-D (working electrode a in Table S2, ESI) made of varied  $TiO_2$  films with the ML configurations shown in (a). The molecular structure of Z907 dye is indicated in the inset of (c).



**Figure 4.** Photovoltaic characteristic plots of (b) JV curves and (c) IPCE action spectra for devices E-H (working electrode a in Table S3, ESI) made of varied  $TiO_2$  films with the ML configurations shown in (a). The molecular structure of Z907 dye is indicated in the inset of (c).

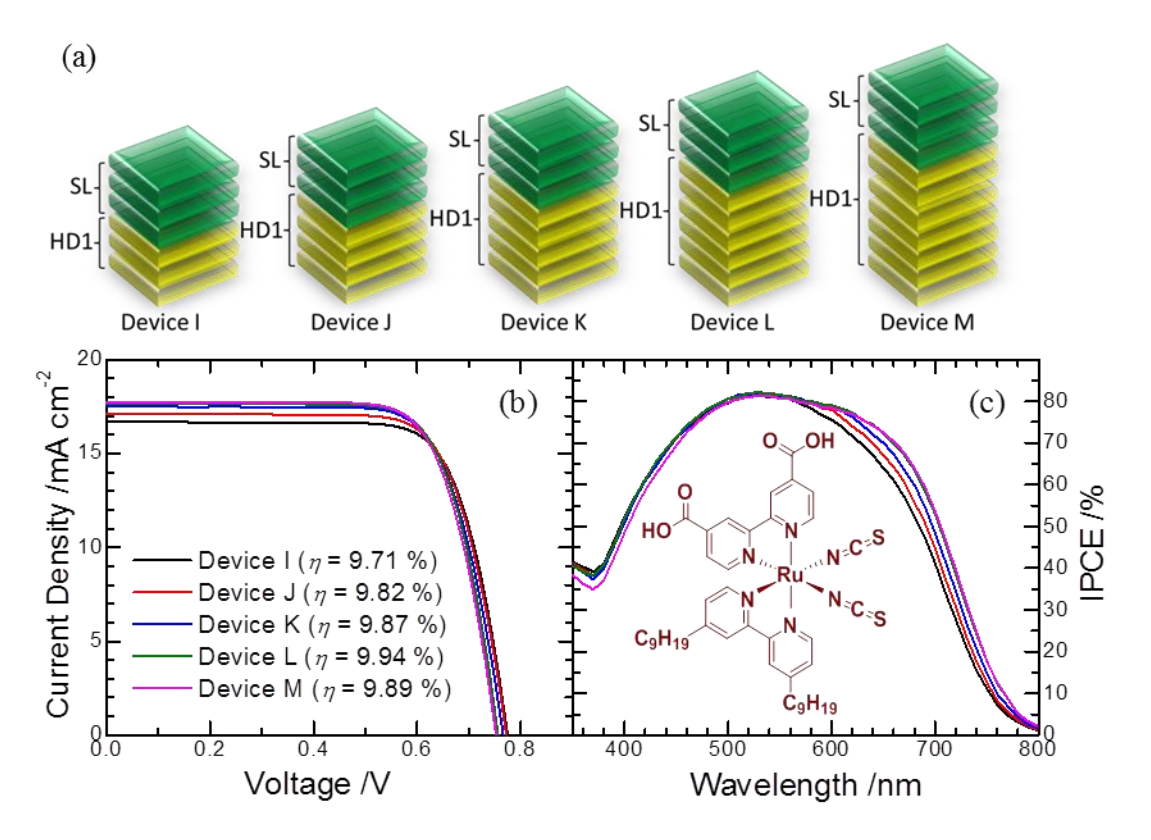


**Figure 5.** Photovoltaic characteristic plots of (b) JV curves and (c) IPCE action spectra for devices I-M (working electrode a in Table S4, ESI) fabricated with TiO<sub>2</sub> films containing a bi-layer (BL) configuration shown in (a). The molecular structure of Z907 dye is indicated in the inset of (c).

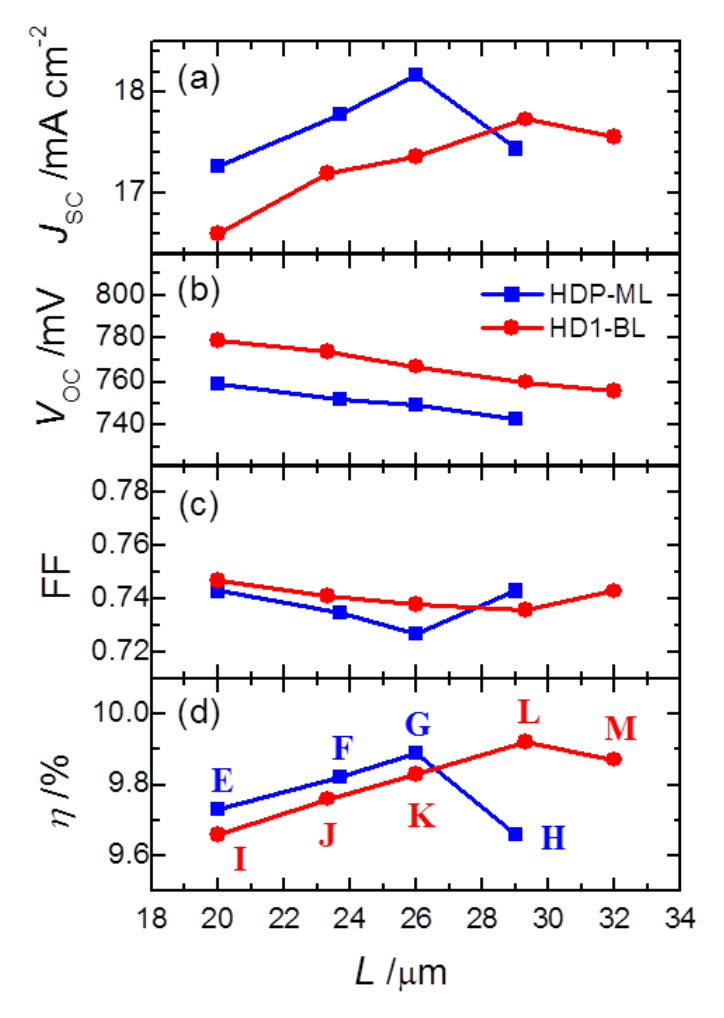


**Figure 6.** (a) Short-circuit current density  $(J_{SC})$ , (b) open-circuit voltage  $(V_{OC})$ , (c) filling factor (FF) and (d) efficiency  $(\eta)$  of power conversion, as a function of total TiO<sub>2</sub> film thickness (L). The results were obtained from the HDP-ML system (filled squares; devices E-H) and the HD1-BL system (filled circles; devices I-M) sensitized with Z907 dye.

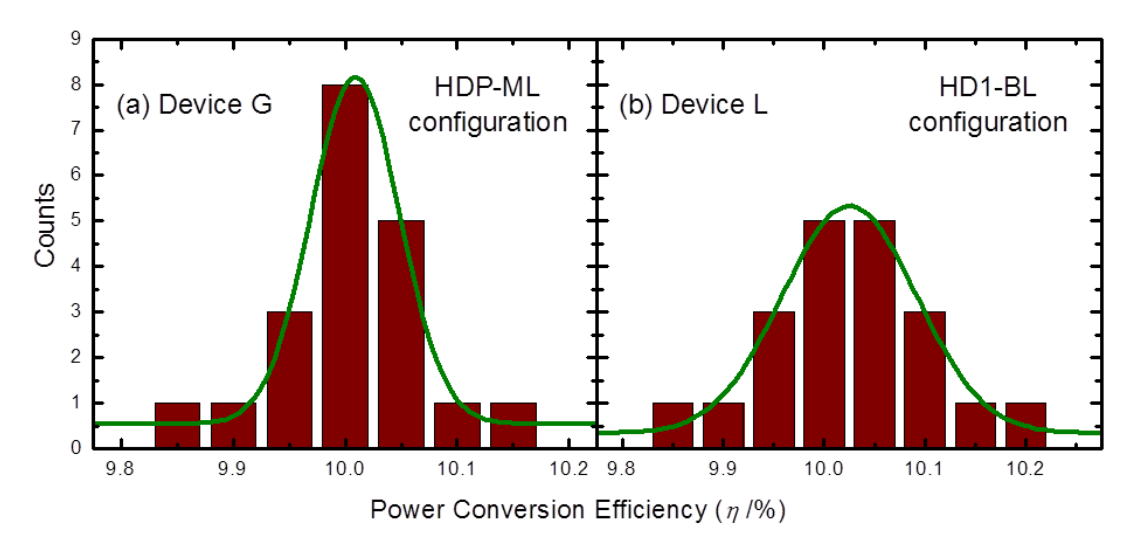


**Figure 7.** Histograms of efficiencies of power conversion (PCE) of 20 devices fabricated under the same experimental conditions with TiO<sub>2</sub> films constructed via the configurations of (a) HDP-ML (device G) and (b) HD1-BL (device L).

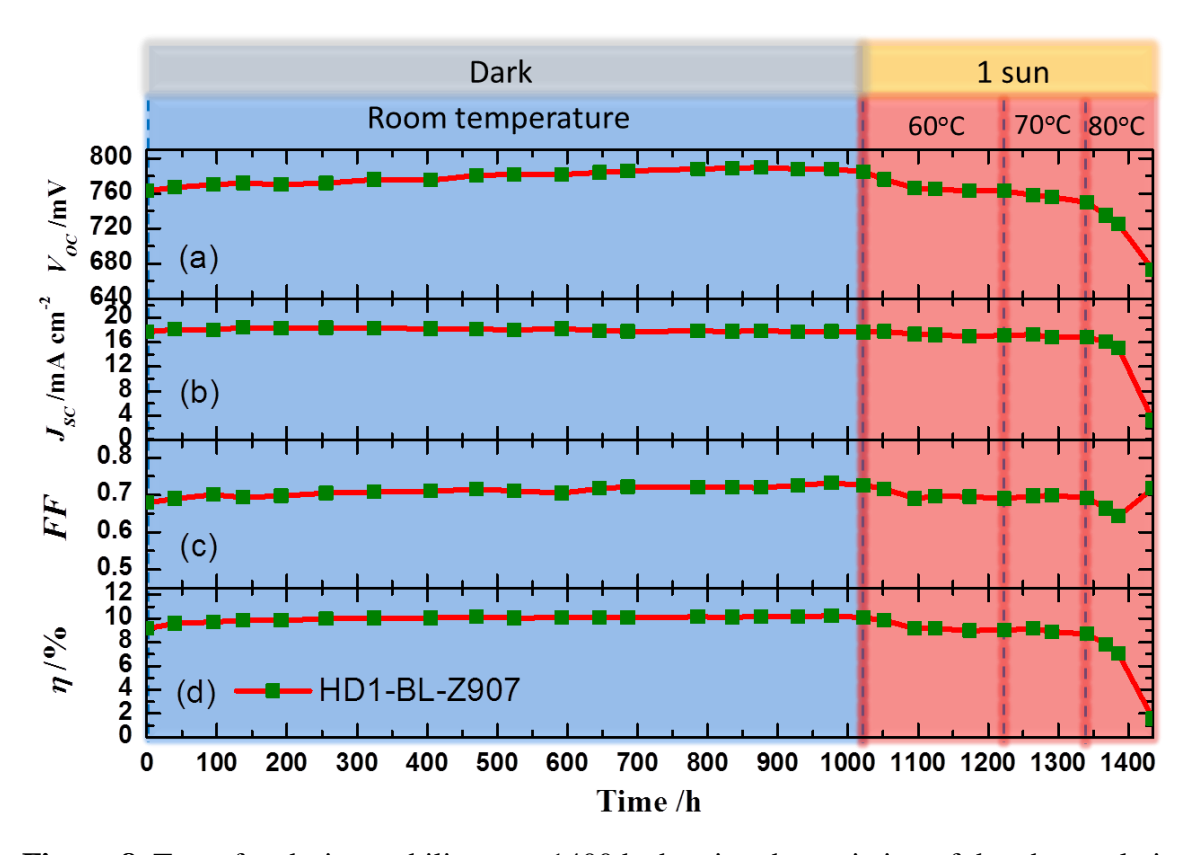


**Figure 8.** Test of enduring stability over 1400 h showing the variation of the photovoltaic performance for (a) open-circuit voltage  $(V_{\rm OC})$ , (b) short-circuit current density  $(J_{\rm SC})$ , (c) filling factor (FF) and (d) efficiency  $(\eta)$  of power conversion for the Z907-based device with a HD1-BL film configuration (device L). The experiments were carried out in darkness near 22 °C for 0-1022h, and then under one sun illumination during periods 1022-1223 h at 60 °C, 1223-1344 h at 70 °C and 1344-1435 h at 80 °C.

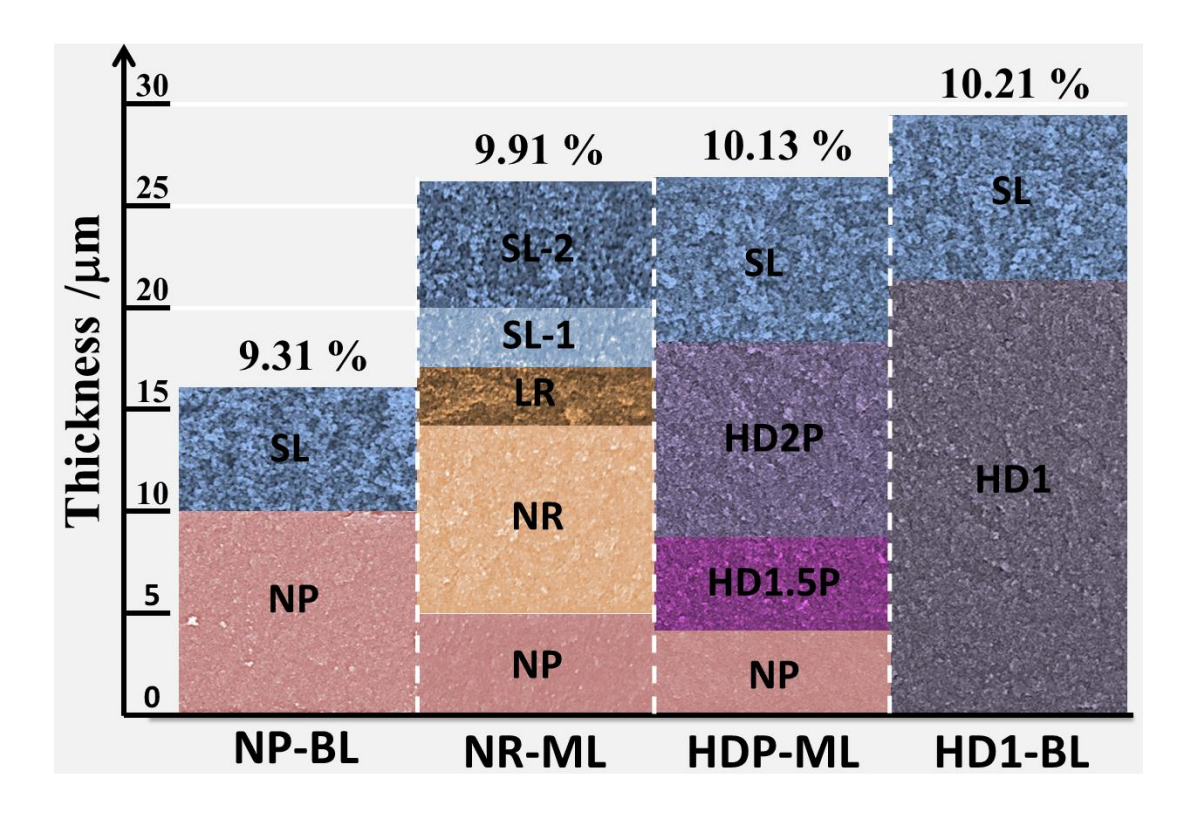


**Figure 9.** Side-view SEM images of TiO<sub>2</sub> films showing each component of film configurations NP-BL, NR-ML, HDP-ML and HD1-BL upon which their device performances were optimized. The scattering layers (SL) in the NP-BL, HDP-ML and HD1-BL configurations are the same as the SL-2 layer in the NR-ML configuration. The values shown above each film are the best PCE of the corresponding devices made of a Z907 dye; PCE of the HDP-ML and the HD1-BL devices are from the present work and those of the NP-BL and the NR-ML devices are adopted from ref. 17.

#### **TOC Entry**

The Z907-sensitized solar cells attained power conversion efficiencies exceeding  $10\,\%$  at the HDP-ML and HD1-BL film configurations.

